A Parametric Study to Improve First Firing Cycle Emissions of a Gasoline Direct Injection Engine during Cold Start

Jinghu Hu*^, Delong Li*^, Matthew Hall**^, Ron Matthews^, Peter Moilanen+, Steven Wooldridge+, Jianwen Yi+
*Co-first authors
**Corresponding author
^Department of Mechanical Engineering, University of Texas at Austin
+Ford Motor Company

Abstract

A parametric study was carried out for the first firing cycle of a 4-cylinder, 2.0-liter, turbocharged gasoline direct injection (GDI) engine. The primary goal was to see how changes in the fuel injection parameters would affect the GDI engine combustion and emissions for the first four combustion events that constitute the first firing cycle. Experimental studies were carried out with a custom-designed powertrain control system to measure the HC emissions and pressure development for the first firing cycle. The quantitative experimental results were accompanied by simulations of the detailed temporal and spatial fuel concentration profiles using Converge CFD engine simulation software. An alternative calculation method was used to calculate the average combustion equivalence ratio for each of the 4 cylinders. This method showed that the majority of the cold start HC emissions during the first firing cycle was unburned gasoline and its possible decomposition products, which did not contribute significantly to the combustion and heat release. For the same amount of fuel injected into a cylinder, increased fuel rail pressure resulted in better evaporation and combustion, while slightly increasing the HC emissions during the cold start process. A multiple injection strategy was studied that split the fuel delivery between the intake stroke and the compression stroke with either one or two injections in each of those strokes (2 or 4 injections total). The quadruple injection strategy led to better first cycle combustion, with higher engine IMEP and lower HC emissions. This resulted from a richer fuel mixture in the region near the spark plug due to better fuel evaporation and a better spatial fuel distribution. While increasing fuel rail pressure with either injection strategy failed to significantly lower the HC emissions given the same amount of injected fuel mass, higher rail pressure with the quadruple injection strategy resulted in higher IMEP for the same amount of injected fuel; this may provide the possibility to reduce the total fuel injection mass which may have benefits for both fuel consumption and emissions.

Introduction

The more stringent HC emissions regulations put in place by the United States Environmental Protection Agency and California Air Resources Board lowered allowed unburned hydrocarbons (HC) by 65% under the Tier 3[1] standards that go into effect in 2025. Having multiple advantages compared with traditional port fuel injection (PFI) engines, due to the capability for cycle-by-cycle fuel injection controls[2], gasoline direct injection (GDI) has steadily gained market share among light-duty vehicles. Its share among model year light-duty vehicles has risen from 2.3% in 2008 to 57% in 2020[3]. With its increasing popularity among vehicle manufacturers, gasoline direct injection engines are under intensive research to reduce HC emissions during the cold start processes[4]. During a typical cold start, a GDI engine is faced with in-cylinder wall temperatures much lower than optimal for good evaporation and experiences rapid changes in engine speed

and fuel rail pressure within the first 5 firing cycles. Further, it is usual to retard the spark timing as soon as possible to enter catalyst-heating mode with lower output IMEP as one cost[5,6]. The lack of hot exhaust residual on the first firing cycle plus low initial and swiftly increasing cylinder wall and piston top temperature[7,8], fuel rail pressure[9,10], the difficulty in estimating trapped air charge due to rapidly varying manifold pressure, and engine speed all contribute to the suboptimal fuel evaporation, non-ideal combustion and high HC emissions. It is thought that the factors above lead to HC emissions mainly by surface impingement of liquid fuel, deteriorating the overall combustion performance and allowing the fuel trapped on the walls to be released at the end of the combustion to form engine-out emissions of HCs[11]. It has been found that the first 5 firing cycles, especially the very first cycle, where most of the engine speed and fuel rail pressure transient takes place, have the greatest contribution to HC emissions[12]. Also, creating the desired equivalence ratio in each cylinder during this transient period is difficult. These issues lead to the current challenges to meet future HC emissions regulations[13].

Multiple research studies, focusing on experimental and simulation methods, have been published in the field of GDI engine cold start. Fan et.al studied the influence of a series of injection parameters, including injection timing and injection split ratios, on the engine energy release performance for the first cycle[14] and on the engine emissions over first 10 firing cycles[15]. Rodriguez et.al. examined effects of fuel rail pressure, cranking engine speed, spark ignition timing, manifold air pressure, and the injection mass on the engine fuel evaporation and engine-out emissions for the first one[13,16] and three firing cycles[17]. They also studied the influence of valve timing on the engine emissions during cold crank start[18]. Malaguti et al.[19] carried out numerical simulation methods to analyze the fuel evaporation and fuel film formation process in the first two firing cycles. Previous research from our research group proposed[12] and validated[20] a novel experimental technique that quantified engine-out emissions for each of the first 5 firing cycles. In addition, a simulation model that focused on the transient engine speed and fuel rail pressure on in-cylinder injection parameters and combustion was used to gain additional insights, as well[21]. Ravindran et al. developed a modified G-Equation combustion model which performs well for the lower Reynolds number regimes under cold-start conditions with constant engine speeds around 1200 RPM[22]. They later utilized an advanced Gaussian process regression (GPR)-based machine learning techniques to predict engine performance for a DISI engine under cold-start conditions.[23] All the research mentioned has shown that improving the combustion performance of the first firing cycle of GDI engine cold starts can not only reduce the HC emissions, but also shorten the time required for the engine to reach the targeted operating conditions at which the catalyst-heating mode of operation becomes possible.

In the present research, a parametric study was conducted to determine how different powertrain cold start configuration parameters affect the GDI engine cold start emissions and combustion performance for the very first firing cycle of all four cylinders. The parameters of interest include injected fuel mass, fuel rail pressure (FRP), different injection strategies (2- or 4-injection strategy), injection fuel mass split ratio (early-late split ratio) between intake stroke (early) and compression stroke (late) injections, and the injected fuel mass split ratio between the two late injections (late-late split ratio) for the 4- injection strategy. The results drawn from experiments were further supported with a validated CFD simulation model, which provided further insight into the fuel temporal and spatial distribution within the cylinder during the intake and compression strokes of the first firing cycle.

Methods and System Setup

Engine Specifications

The engine used for the present study was a 4-cylinder, 2.0-liter gasoline turbocharged direct injection engine. The variable valve timing was disabled, and by default the intake valve remains at full retard and the exhaust valve at full advance. The turbocharger was in place but not active during the experiments. The engine was a direct injection engine, with the injector nozzle located between the two intake valves. The engine is also solely GDI, i.e., no additional PFI fuel system is present. During cold starts, the piston top plays a significant role in deflecting air and injected fuel, and thus fuel vapor, toward the spark plug. Hence, piston top wall wetting can be strong and a detailed tuning of the injection timing is needed to minimize HC emissions during the first firing cycle. A more detailed list of engine specification is shown in Table 1.

Table 1 Engine Specifications

Displacement	1999 cc
Bore/Stroke	87.5 mm/83.1 mm
Connecting Rod Length (Center to Center)	155.9 mm
Compression Ratio	10:1
IVO/IVC	10.9° ATDC/71.1° ABDC
EVO/EVC	55.1° BBDC/5.1 ATDC
Firing order	3-4-2-1
1st cycle spark ignition	10° BTDC
Baseline idling speed	1200 RPM
Baseline Intake Valve	Fully Retarded
Baseline Exhaust Valve	Fully Advanced

Experimental System Setup

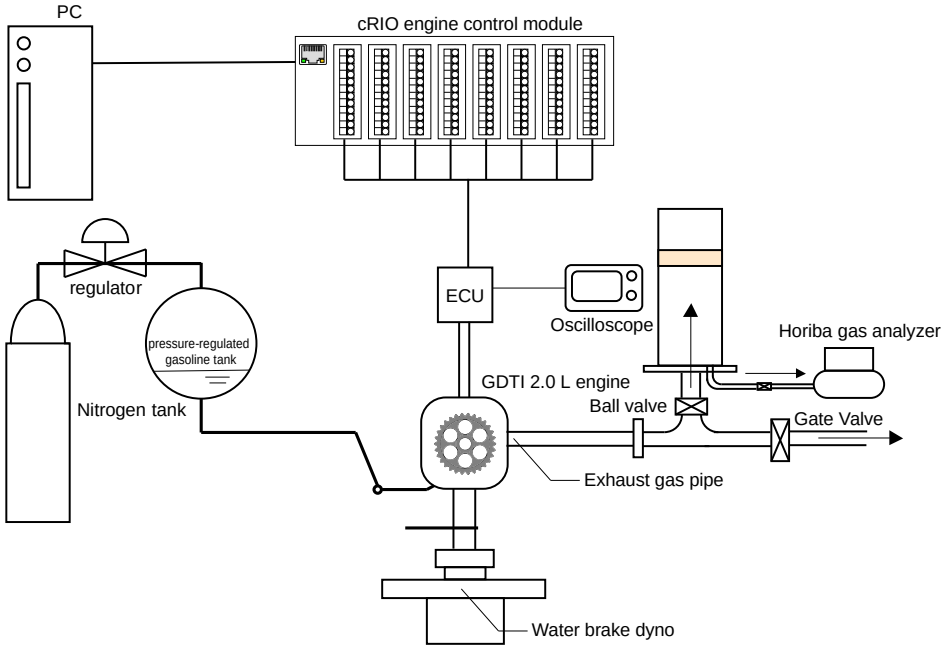

Figure 1 Experimental schematic

The experimental system schematic is shown in Figure 1. The entire system was placed in an environmental chamber whose temperature was controlled to 22±1 °C (295±1 K) throughout the experiments. A water brake dynamometer was connected to the engine flywheel to provide load similar to a typical engine cold start. A custom engine ECU was configured using National Instruments cRIO hardware. Seven individual NI control modules connecting relevant vehicle control and sensor pinouts, were assembled onto a NI cRIO-9048 chassis connected to the host PC via an Ethernet connection. A custom-developed NI Real-Time-FPGA control program was deployed to control the engine and log the operating data. Two Siglent SDS1104X-E 4-channel oscilloscopes were connected to the 4 Kistler 6125A in-cylinder piezoelectric pressure transducers which detected the instantaneous cylinder pressure of each cylinder. The oscilloscopes were also connected to the signal output of an incremental rotational encoder, which was fixed onto the crankshaft and had an angular resolution of 0.5 degrees. The logged temporal engine pressure trace data not only provided engine cycle quantification by displaying the number of cycles the engine elapsed, but also, with the aid of temporal engine position data provided by the incremental encoder, allowed crank angle-based engine cycle analysis, including IMEP calculation and heat release calculation.

To eliminate the transient effect of the normally rapidly increasing fuel rail pressure during cold start, a titanium spherical tank containing standard E10 gasoline was directly connected to the common fuel rail, bypassing the deactivated high-pressure fuel pump on the engine. A nitrogen tank was connected to the upper end of the titanium tank via a regulator. The adjustment of the regulator allowed for the fuel inside the titanium tank to be controlled to a specified pressure level which, in turn, maintained the fuel rail pressure at a constant, user-specified, value.

A gas collection volume (GCV) was placed downstream of the exhaust manifold along with a two-way exhaust pipe system. The exhaust gas coming from the exhaust manifold was directed into the GCV when the ball valve between the volume and the main pipe was opened and the gate valve between the main pipe and the building exhaust system was closed. The GCV was a 1 m tall, 19 cm inner-diameter acrylic cylinder, with a plastic foam piston sealing the cylinder. A Horiba MEXA-554JU gas analyzer was connected to the bottom of the GCV through a 3/8'' NPT pipe fitting. Before each gas collection and measurement process, the gate valve would be shut and the ball valve would be opened. During the cranking or the cold start process, the exhaust gas would be guided into and trapped inside GCV, then the gas volume was measured, and the gas composition analyzed with the gas analyzer to obtain HC (in hexane base), CO, and CO_2 molar concentrations.

Powertrain Parameters of Interest

The main parameters of interest within this study were the injected equivalence ratio (or injected fuel mass), the delivery fuel rail pressure, and the injection strategy. In the quadruple injection strategy, the fuel injection split ratio between the early (intake stroke) and late (compression stroke) injections and the fuel injection split ratio between the two late injections during the compression stroke affected the fuel distribution and evaporation. To carry out the parametric analysis, a baseline parameter set was established, and the corresponding engine performance and emissions were measured. From this baseline, a series of parametric sweeps of each parameter was carried out. The results were then compared with the baseline results to qualitatively and quantitatively understand whether the variation of the parameter achieved performance improvement, and what parameter set would lead to the optimal engine performance and emissions results.

A detailed introduction of all the powertrain parameters studied is provided below.

- *Injected equivalence ratio (ϕ_i)* The injected equivalence ratio was the key variable affecting the fuel evaporation, combustion, and exhaust gas emissions. For a warmed-up engine at operating temperature, the injected fuel mass is adjusted to keep combustion near stoichiometric via closed-loop control. However, it is not possible to establish fast closed-loop control during a cold start before the oxygen sensor becomes active. Understanding how the injected equivalence ratio affects the combustion and emissions of the first firing cycle was necessary. The overall injected equivalence ratio for the baseline scenario was set to be 1.14, with a slightly richer equivalence ratio of 1.26 for cylinders 3 & 4, which were the first and second to fire, and 1.02 for cylinders 2 and 1, which were the third and last to fire, respectively. An injected equivalence ratio sweep was carried out during the experiments. During the injected equivalence ratio sweep, the injection duration ratio among the 4 cylinders remained unchanged.
- *Fuel rail pressure (FRP)* Gasoline was delivered to the injectors via the common fuel rail. In this study, the baseline fuel rail pressure was set to 80 bar. Higher fuel rail pressures (up to 120 bar) and lower fuel rail pressures (60 bar) were also used to study the effects of FRP. Higher fuel rail pressures result in smaller Sauter mean diameter droplets, enhancing mixing with the in-cylinder air, promoting evaporation with less fuel

wall wetting. Higher FRP also reduced the injection duration necessary to achieve the same amount of injected fuel mass.

- *Injection strategy* Common rail fueling and in-cylinder electrically controlled high pressure injectors have made multiple injections within one cycle possible. A common practice for the first few firing cycles, when engine load is low and conditions for ignition challenging, is to create a stratified fuel-air mixture. A typical strategy is a 2-injection strategy with one injection during the intake stroke to form a lean fuel-air mixture, then one injection during the compression stroke to achieve a combustible mixture around the spark plug. The effect of additional injections on engine performance was explored. In this study, the baseline was a 2-injection strategy, with intake injection starting at 220 crank angle degrees (CA^o) BTDC and compression stroke injection ending at 45 CA^o BTDC of compression. For comparison, a quadruple injection strategy was used, with 4 injections, 2 during intake and 2 during the compression stroke. By default, each of these injections injected exactly the same amount of fuel, indicating a 50%-50% early-late split ratio and a 50%-50% late-late split ratio for the late, compression stroke, injections. The two intake stroke injections started at 240 and 200 CA^o BTDC respectively. The two compression stroke injections ended at 55 and 35 CA^o BTDC, respectively.
- *Early-late split ratio (ELSR) and late-late split ratio (LLSR) with the 4-injection strategy* During the first firing cycle of the cold start, a common practice is to carry out injections in both the intake stroke and compression stroke to create a spatially stratified fuel distribution. The purpose of this practice is to increase the probability of a combustible mixture at the spark plug. While late injection(s) were essential to guarantee a robust firing of the cylinders, not all of the fuel injected during the compression stroke will vaporize; the rest either remaining liquid in the cylinders before either entering the crankcase or evaporating late in the expansion or exhaust stroke to exit as HC emissions. When the 4- injection strategy was used, the 2nd late injection, whose injection timing was pushed even closer to the time of ignition, suffered from even poorer evaporation. The fueling default was that the early-late split ratio was 50%-50% for both the 2-injection and 4-injections cases while the baseline split ratio, between the two late injections for the 4-injection cases was also 50%-50%, indicating equal amounts of fuel injected per each injection. Since the engine injectors were linear in their fuel delivery for injection durations greater than 0.6 ms, the default FRP was set to 60 bar to allow longer injection durations, and only durations greater than or equal to 0.6 ms were used.

A brief summary of the parameters studied in this research is listed in Table 2.

Table 2 Powertrain parameters studied in this research

Powertrain parameters	Baseline configuration	Other configurations
Injected equivalence ratio (ϕ_i)	1.14 overall 1.26 for cylinders 3 & 4 1.02 for cylinders 2 & 1	0.8~1.6 of baseline ϕ_i
Fuel rail pressure (FRP)	80 bar	120 bar; 60 bar
Injected strategy	2-injection strategy: 1 injection at intake stroke; 1 injection at compression stroke	4-injection strategy: 2 injections at intake stroke; 2 injections at compression stroke

ELSR for 4-injection strategy	50%-50%: equal injected fuel mass between 2 early injections and 2 late injections	60%-40% 70%-30%
LLSR for 4-injection strategy	50%-50%: equal injected fuel mass between two late injections	60%-40% 70%-30%

Experimental Process

How each experimental case was carried out and the data collected is shown in Figure 2. Before each experiment the engine soaked for at least 12 hours in the environmental chamber to make sure the temperatures of the cylinders, coolant, and components were all restored to 22 ºC. Prior to a fueled cold start, the engine went through 5 pre-cold start cranking measurement periods; each measurement consisting of 14 engine cycles and having an interval of 4 minutes apart from its predecessor. The HC emissions of each of these 5 measurements were analyzed. The objective of the 5 pre-cold start cranking measurements was to quantify the potential background HC sources inside the cylinder. The average of the obtained per-cycle HC emissions through the 5 pre-cold start cranking measurements was calculated and treated as the background HC emissions level.

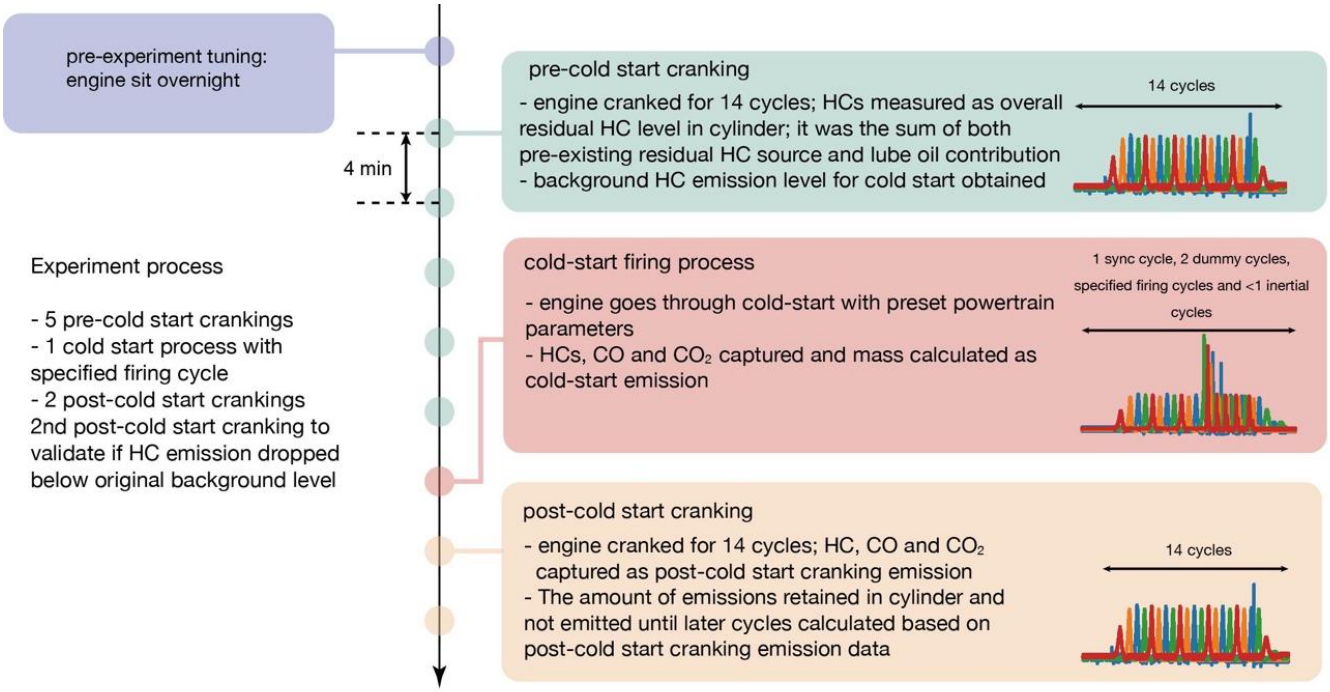

Figure 2 Experimental process

Four minutes after the last pre-cold start cranking event, a cold start firing lasting for 1 firing cycle was carried out with all preset parameters. During the cold start firing, the engine first went through 3 dummy cranking cycles, without fuel injection, for engine position synchronization. After the 3 dummy cycles, 1 firing cycle followed where the spark ignition and

fuel injection were activated. After the firing cycle, all powertrain components were deactivated, and the engine went through a short inertial slow-down (usually <1 full cycle) before coming to a stop. The exhaust gas throughout all these cycles was trapped inside the GCV before being sampled and analyzed. The collected HC mass from the single cold start cycle was defined as the cold start HC emissions of the first firing cycle, and was the main focus of this study.

The cold start firing process was followed by 2 post-cold start cranking measurement periods. Like the pre-cold start cranking events, the engine went through 14 cycles for each, with the two events separated by 4 minutes. HC, CO, and CO_2 emissions were measured and emitted masses calculated. The objective of the post-cranking was to quantify the emissions generated during the cold start firing but not recovered until later cycles, possibly due to late evaporation of liquid fuel. The CO and CO_2 emissions collected via the post-cold start cranking processes were summed up with the emissions collected during the cold start firing process. The summed CO and CO_2 emissions masses were treated as the cold start CO and CO_2 emissions respectively. The justification for this processing method was that there should be no generation of CO and CO_2 during pure post-cold start cranking, and indeed, the only CO and CO_2 collected, post cold start, was for the very first post-cold start cranking event where there was some residual recovered from the exhaust manifold. That observation validated the assumption. All captured emissions were used to calculate the fuel mass that was not collected at the end of the post-cold start cranking process. The uncollected portion of the injected fuel was treated as the fuel not evaporated during the process, and presumably, lost to the crankcase past the rings.

Indicators of Interest

The cold start HC emissions were of primary interest in this study. While the HCs emitted during the post-cold start cranking events were essential to quantify the carbon element balance between injected and emitted fuel, it did not share the same significance as the cold start HC emissions with respect to tailpipe emissions, as most of these later emitted HCs would be combusted in later cycles in real engine cold starts. The uncollected portion of the injected fuel was also given great attention. This portion of the fuel not only contributed to the fuel economy loss, but also served as a potential source of the HC emissions in the later cycles. Reducing this unevaporated, uncollected portion of the injected fuel was another focus of this study.

Apart from the emissions and fuel economy indicators, two other parameters were also of interest: the average engine indicated mean effective pressure (IMEP), and overall combusted equivalence ratio (ϕ_c, as distinguished from the injected equivalence ratio ϕ_i). Average IMEP was calculated by processing the time-based pressure traces and encoder data from the oscilloscopes and was a key indicator of engine torque development throughout the first firing cycle.

The difference between ϕ_c and ϕ_i served as a key indicator of the fuel evaporation status, and therefore, the effectiveness of the fuel utilization. Traditionally, the combustion equivalence ratio is obtained by the calculation of the air/fuel ratio from the concentrations of various components in the exhaust gas. Such a set of concentration data was unavailable due to the experimental design and an alternative method was used to calculate the actual combusted mixture fuel/air ratio and hence combusted equivalence ratio. For this calculation, the masses of

the major emitted species were calculated based on the analyzer concentrations and the combusted equivalence ratio was calculated on a mass basis. It was assumed that the emitted HCs did not participate in the combustion reactions, and therefore did not contribute to the combusted equivalence ratio. Effectively, the emitted HCs were taken to be from gasoline evaporation instead of from incomplete combustion reactions and were ignored in the combusted equivalence ratio calculation. A more detailed presentation of the alternative method is shown in the appendix.

Numerical simulation methods

Three-dimensional simulations for the very first firing cycle were carried out with CONVERGE CFD™ version 3.0, a CFD package widely used in engine simulations. The standard combustion model within Converge was replaced with a fractal engine simulation (FES) model, implemented as a user define function (UDF). The FES model solves the turbulent combustion in an engine in a more physically meaningful way: it assumes that the dominant effects of turbulence on combustion are to winkle and stretch the flame surface so that the turbulence accelerates the combustion process. Thus, a fractal dimension is employed to calculate the turbulent burning velocity, accounting for the increase in the surface area of the flame. Besides the FES model, different models such as the turbulence model, injection model, and wall film model were all included in the simulations. A transient engine speed, obtained from the experiments, was used in the simulations to better represent the actual event in the very first firing cycle during the cold start process. As the simulation was not the main focus of this paper, its details can be found in prior publications that describe the FES model[24] and our application of Converge CFD[21]. A detailed overview of the numerical simulation model is presented in Table 3.

Table 3 Numerical simulation models introduction

Process	Model	Details
Combustion	Fractal Engine Simulation	Integrated into the 3D engine simulation as a user-define function (UDF) in CONVERGE.
Spray breakup	Modified KH-RT model	Model constants: KH size constant B_0: 0.6; KH time constant B_1: 7.0; RT size constant C_{RT}: 0.6; RT time constant C_τ: 1.
Spray-wall interaction	Wall film model	Critical Weber number We_{cric}: 5.0; Critical value for splashing E^2_{cric}: 3330; Fraction splashed: 1.0.
	O'Rourke model	
Fuel	Iso-octane	Kinetics from reference 25
mesh	Fixed embedding	Base grid size: 4 mm. Fixed embedding: level 2 for cylinder; level 3 for spray; level 5 for ignition. AMR: level 3 using the sub-grid (SGS)-based type for temperature and velocity; boundary AMR included as well, for valves as an example.
	Adaptive mesh refinement (AMR)	

Results and Discussion

Engine speed and pressure trace results

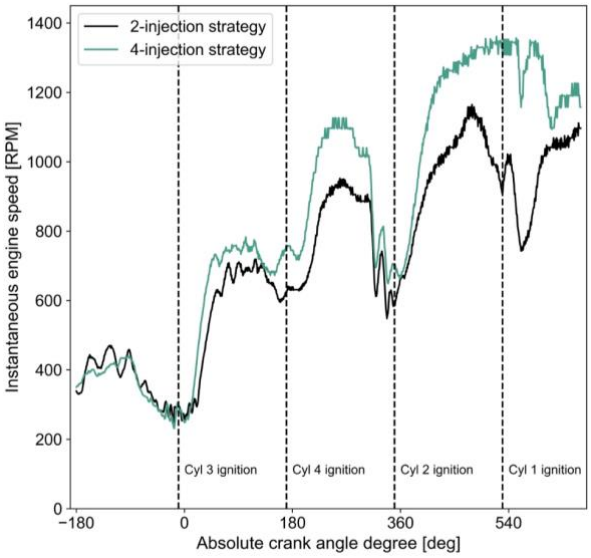

Figure 3 Typical instantaneous engine speed profile within the first firing cycle

The instantaneous engine speed for the first firing cycle is plotted in Figure 3. The 0 absolute crank angle degree shown in Figure 3 represents the compression stroke top dead center (TDC) of the first cylinder to fire, i.e., cylinder 3 TDC. The instantaneous engine speed increased shortly after each ignition except in cylinder 1 (the last cylinder to fire), where the instantaneous engine speed dropped before again rising. Each engine speed increase raised the engine peak speed, propelling the engine speed to reach approximately 1200 RPM (1300 RPM for the 4-injection strategy discussed later) at the end of the first firing cycle. The 4-injection strategy achieved consistently higher engine speeds compared with the 2-injection strategy.

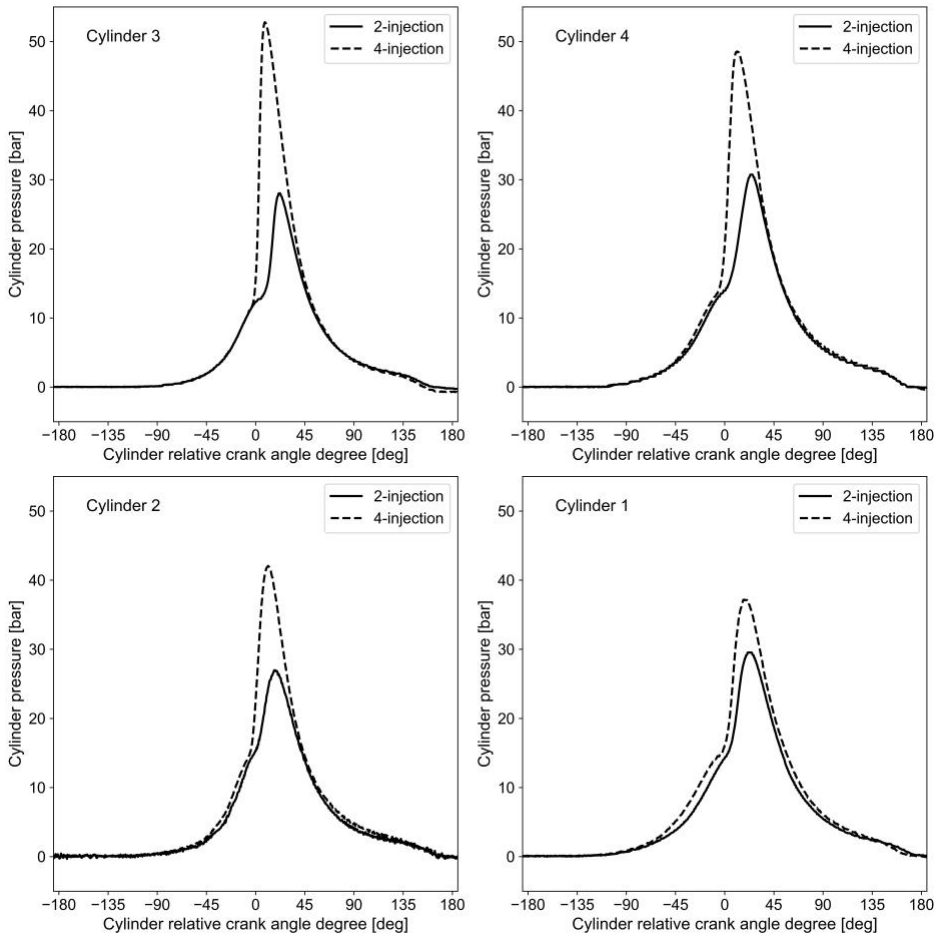

Figure 4 Cylinder pressure profiles for the first firing cycle with 80 bar of FRP

A typical cylinder pressure profile displaying the pressure trace of each cylinder during their first firing event is shown in Figure 4. The peak pressure of the same cylinder was significantly higher when the 4-injection strategy was used. The improvement of peak pressure with the 4-injection strategy was a key finding of this work and will be discussed in detail in the paragraphs below. In the 4-injection scenario the cylinder peak pressure was lower for each successive firing event in the first cycle; cylinders firing later had lower peak pressure compared with cylinders firing earlier. Such a trend was not true for the 2-injection scenario. The difference might be due to the engine speed profile difference displayed above.

ϕ_c and HC emissions results

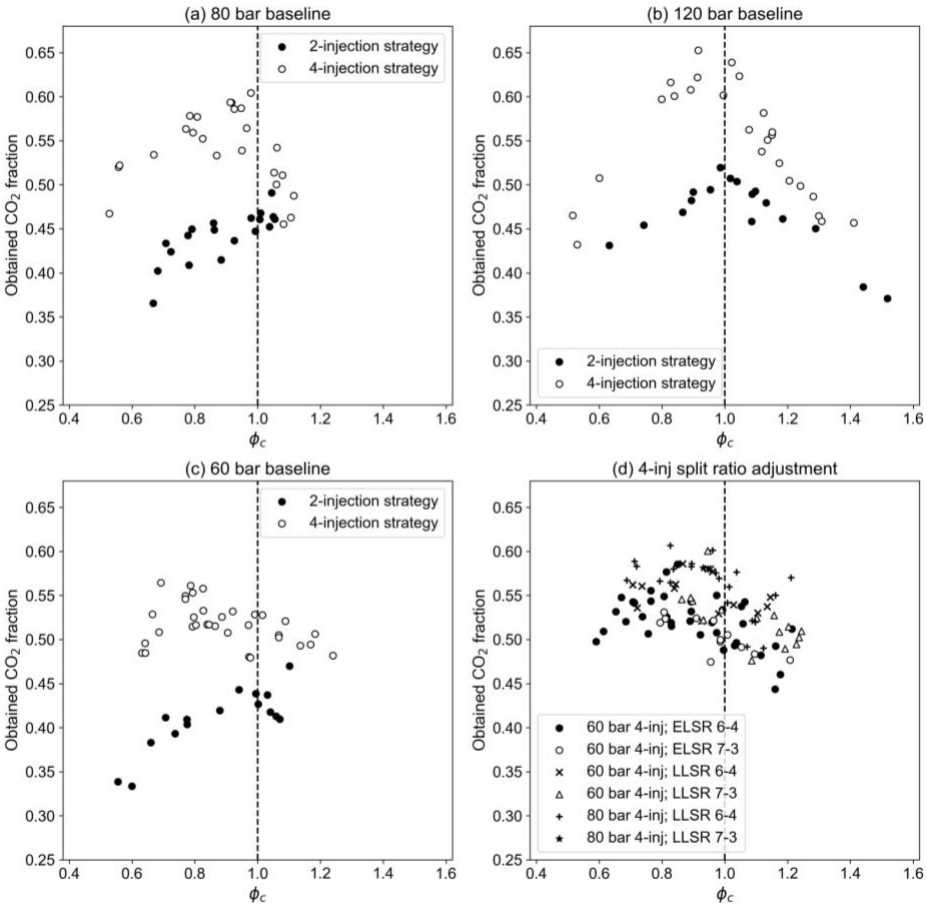

Figure 5 CO_2 carbon mass fraction with change of calculated combusted equivalence ratio

The combusted equivalence ratio ϕ_c was calculated without considering the collected HC emissions, since this unburned fuel did not contribute to the combustion. To justify this approach, the mass of carbon collected from the CO_2 was normalized by the total injected fuel carbon mass and plotted against the calculated ϕ_c for each powertrain parameter group. Historically and theoretically, combustion research has found that the CO_2 concentration peaks when ϕ_c is close to stoichiometric. It can be seen from Figure 5 that the emitted CO_2 portion of carbon peaked at around combustion stoichiometric for each group of powertrain parameters, despite outliers. Such a trend was more obvious in the 2-injection strategy data and baseline 4-injection strategy, while larger fluctuations of the data were observed when using the non-baseline early-late and late-late split ratios for the 4-injection strategies. If cold start HC emissions were taken into consideration when calculating ϕ_c, the location at which the emitted CO_2 percentage peaked was approximately 1.2 of ϕ_c, demonstrating that the current method to leave out HC emissions when calculating ϕ_c was reasonable. Thus, for the first firing cycle, the majority of emitted HCs did not participate in the combustion reactions, and hence it was assumed that the HC emissions consisted primarily of the non-combusted gasoline (or its decomposition products). The previous conclusion further implied that one should be able to reduce the first firing cycle emitted HCs by improving the gasoline evaporation and/or the extent

of combustion and minimizing the amount of injected gasoline that evaporated late and did not take part in the combustion.

Besides the validation of the combusted equivalence ratio, the percentage of the injected carbon converted to CO_2 also reflected the success of the cold start combustion. A higher conversion rate to CO_2 indicated better evaporation and less fuel loss to liquid films. An important trend from this graph is that increasing fuel rail pressure and switching from double injection to quadruple injection helped achieve somewhat better fuel evaporation and more complete combustion as indicated by higher CO_2 concentrations for a given combusted equivalence ratio. The adjustments of the ELSR and LLSR from baseline values with 4-injections did not show a significant increase in the conversion rate to CO_2, implying that those approaches did not achieve much improvement for the cold start first cycle combustion.

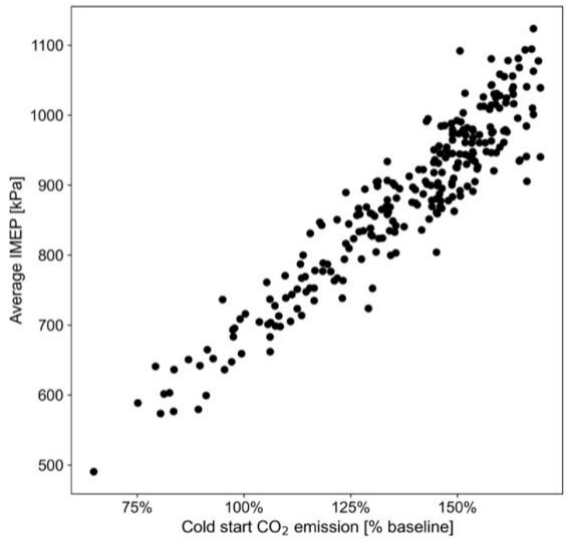

Figure 6 Average IMEP with change of emitted CO_2 mass

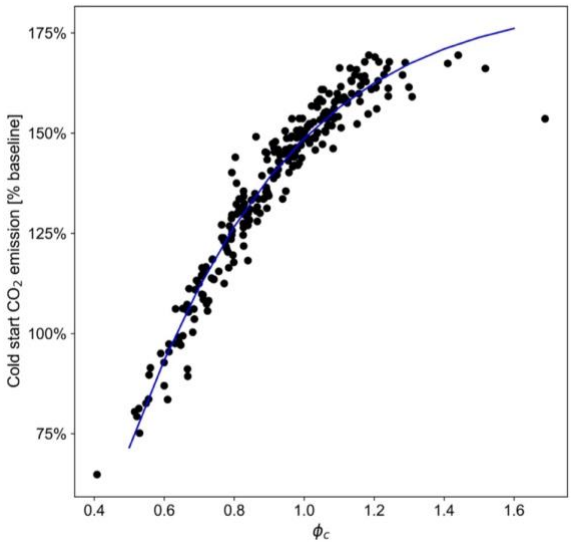

Figure 7 Cold start emitted CO_2 with change of combusted equivalence ratio

The significance of ϕ_c is that it had a good correlation with the emitted CO_2 mass as well as average IMEP, two indicators strongly relevant to the pressure development and torque output. The change of the average IMEP with the increase in emitted CO_2 mass is plotted in Figure 6, and the emitted CO_2 mass change with increasing ϕ_c is plotted in Figure 7. From Figure 6, a clear linear positive correlation between CO_2 mass and the average cylinder IMEP was observed, indicating that the conversion from gasoline fuel to CO_2 was the major source of released energy, as expected, and that the increasing the IMEP was the result of the increasing amount of fuel converted to CO_2. Figure 7 shows that as ϕ_c increased, CO_2 emissions and IMEP increased strongly until ϕ_c approached 1.2. When ϕ_c increased beyond 1.2, CO_2 and average IMEP did not further increase significantly. That is because when the air-fuel mixture was rich, the excess fuel was not fully oxidized from CO to CO_2, and little extra IMEP could be extracted from this reaction. In addition, an excessively rich air-fuel mixture might have inhibited fuel evaporation, making the air-fuel mixture less favorable towards stratified combustion compared with that in lean or slightly-rich air-fuel scenarios. These results show that the mass of fully combusted gasoline was the main contributor to the IMEP during a firing event, and that ϕ_c is a good indicator of the amount of fuel achieving complete combustion. While the fraction of injected fuel converted to CO_2 peaked near ϕ_c equal to stoichiometric as shown in Figure 5, increasing ϕ_c yielded additional CO_2 and increasing IMEP until ϕ_c reached 1.2, as represented by Figure 7 (note that IMEP increased linearly with CO_2).

From a fuel economy standpoint and for emissions optimization, it was desirable to maintain overall cylinder ϕ_c near 1.0, while minimizing over-fueling. However, in scenarios where extra IMEP may be required, maintaining ϕ_c at approximately 1.2 gave maximum starting torque. These results also support the previous discussion concluding that emitted HCs did not contribute significantly to the heat release, and that emitted HCs probably consisted mainly of unburnt gasoline or its decomposition products.

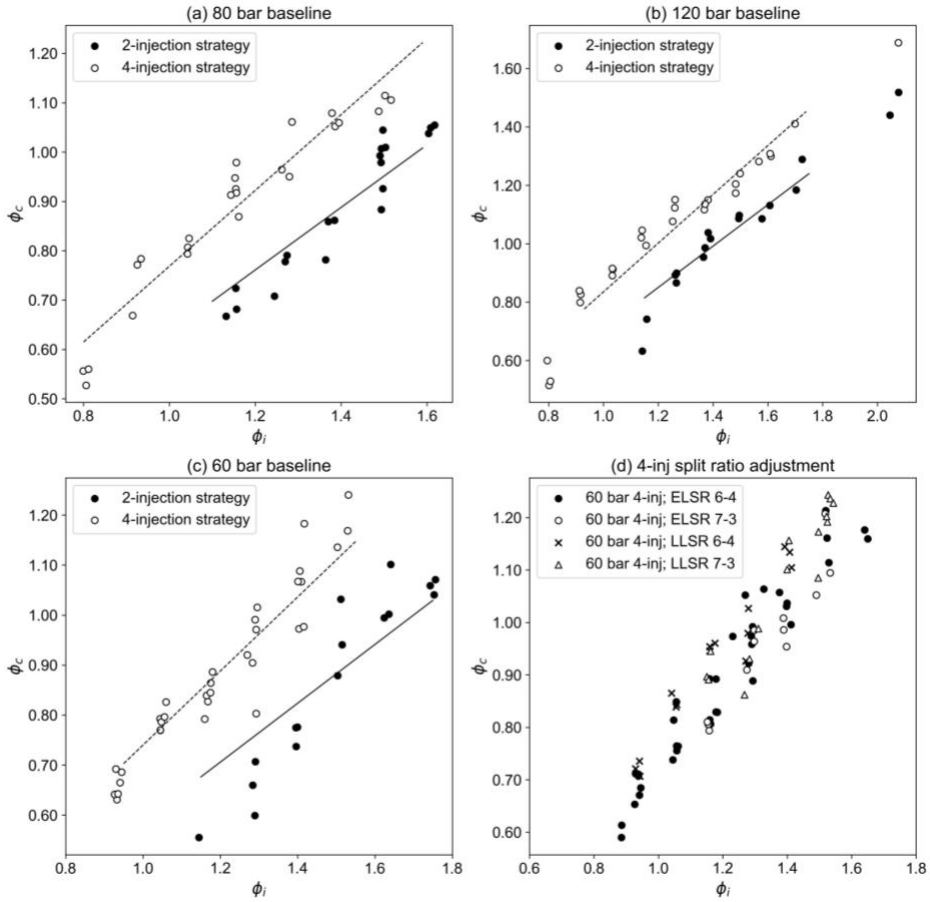

Figure 8 Combusted equivalence ratio change with injected equivalence ratio

The change of ϕ_c with ϕ_i, for different fuel rail pressures and fuel split ratios is shown in Figure 8. In Figure 8, the comparison between the 2-injection strategy and the baseline 4-injection strategy results are plotted for 80 bar, 120 bar and 60 bar in (a), (b) and (c), respectively. In subplots (a), (b) and (c), the results were fitted using an ordinary least square (OLS) linear regression with the intercept forced to be 0. The results of the adjusted ELSR and LLSR are shown in (d), without OLS fitting. In general, ϕ_c increased with ϕ_i for all the results, and the positive correlations were well fitted using linear regression, with regression R^2 between 0.79 and 0.96. The data points were farther away from the linear fit line when ϕ_i was lower than 1.2 for the 2-injection strategy, possibly due to partial combustion. This trend implies that at a given operating condition, a fixed fraction of the injected fuel mass was evaporated and combusted. The slopes indicate the average combusted fuel fraction for the given operating condition over the range of ϕ_i. A parameter change resulting in an increased slope suggests enhanced fuel vaporization that reduces the non-combusted portion of the injected fuel, with less wall and piston top fuel wetting and less consequential fuel loss.

Increasing fuel rail pressure gave a higher average combusted fuel fraction, i.e., expected ϕ_c given the same ϕ_i. Increasing the FRP from 80 to 120 bar led to ~12% and ~9% increases in overall ϕ_c, for the 2- and 4-injection strategies, respectively. A decrease of FRP from 80 bar to 60

bar led to a ~7% decrease in ϕ_c, for the 2-injection case, but an insignificant change for the 4-injection case. For the first firing cycle of the gasoline engine cold starts, the ambient temperature was low and the fuel rail pressure was low compared with normal operating conditions. Under these conditions, higher FRP leads to smaller Sauter mean droplet diameters and may also enhance mixing via the higher kinetic energy of the spray, which can shorten the time required for full evaporation. Although higher FRP will also lead to increased spray penetration and higher impingement on surfaces, such effects appear to not offset the effect of smaller droplets and improved evaporation.

Switching from a 2-injection to a 4-injection strategy resulted in significant increases in ϕ_c. Switching from the baseline 2-injection strategy to 4-injections increased ϕ_c by ~26%, ~21%, and ~18% for 60 bar, 80 bar, and 120 bar FRP, respectively, for a given ϕ_i. Two shorter duration injections resulted in better vaporization than one longer pulse of the same total fuel mass within the same stroke. This effect is considered further below. Additionally, splitting the injection event into two pulses vs one pulse for the same mass injected also has an effect of reducing overall spray penetration, which can lower fuel impingement on surfaces and thereby increase the mass of fuel available for combustion.

Figure 8 shows that ϕ_c values for either ELSR or LLSR were not significantly different from the 60 bar FRP, 4-injection baseline results. That indicates the relationship between ϕ_c and ϕ_i was insensitive to both ELSR and LLSR for the 60 bar injection pressure at which the measurements were made. Some minor trend were evident: adjusting LLSR from the baseline to 60%-40% and 70%-30% for the 4-injection case resulted in slightly higher combusted equivalence ratios. The 60%-40% LLSR saw an improvement slightly better than the 70%-30% LLSR. However, given the large scattering of the data, such observations should be treated with caution. It appears that finding an optimal late-late split ratio for a given injected mass during the compression stroke can lead to slight engine performance and emissions improvements.

The HC emissions are plotted against ϕ_i for different FRP, injection strategies and ELSR/LLSR in Figure 9. From the results, the cold start HC emissions increased approximately linearly with ϕ_i. Like in the ϕ_c -ϕ_i relationship section, a linear fit using OLS with zero intercept was used, and R^2 were in the range of 0.84~0.93 for 6 baseline fits. The fit line slopes represent the conversion rate of injected fuel to cold start HC emissions. Lower HC-ϕ_i slopes indicate a lower HC conversion rate from the injected fuel, which is desirable.

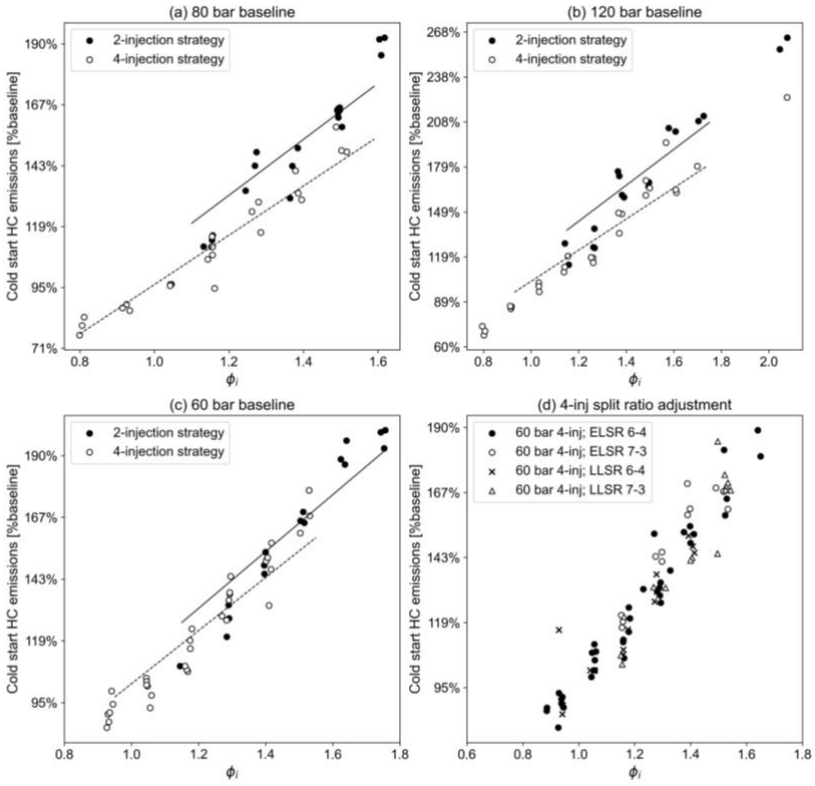

Figure 9 Cold start HC emissions with change in injected equivalence ratio

The HC emissions had a complicated nonlinear trend with injection pressure. For the 2-injection strategy, given the same ϕ_i, increasing the fuel rail pressure from 60 bar to 80 bar did not significantly change the HC emissions, but they increased by ~8.5% when the FRP was further increased from 80 bar up to 120 bar. For the baseline 4-injection strategy, cold start HC emissions decreased when FRP was increased from 60 bar to 80 bar, before increasing again by ~6% back to the original level when FRP was further increased to 120 bar. For certain injection strategies, there exist two offsetting effects on HC emissions from the increase in FRP. While higher FRP improves evaporation and leads to a larger fraction of the fuel combusted, stronger combustion will lead to higher temperatures at the cylinder walls and piston top, causing more wall-wetted fuel to evaporate during and/or after the combustion process and emitted as cold start HC emissions. For the 2-injection strategy, the FRP increase from 60 to 80 bar saw these two effects offset each other, and another FRP increase to 120 bar led to higher HC emissions than 80 bar FRP. For the 4-injection strategy, the FRP increase from 60 to 80 bar resulted in a larger reduction in HC emissions from better evaporation than whatever increase there might have been from late fuel evaporation from higher wall temperatures. The magnitudes of two effects were reversed when FRP was further increased and HC emissions at 120 bar were restored back to the 60 bar FRP level.

Compared with the 2-injection strategy, the baseline 4-injection strategy had lower cold start HC emissions for the same mass of the injected fuel. For fuel rail pressures of 60, 80, and 120 bar, the cold-start emitted HCs decreased by 6.5%, 11.9%, and 13.4%, respectively, with 4-injections relative to the baseline case with 2-injections. Such a reduction is indicative that the 4-injection

strategy not only increased the mass of fuel combusted, but also reduced the overall residual gas-phase fuel that remained un-combusted throughout the cold start process.

Neither ELSR nor LLSR changes at 60 bar FRP significantly changed the HC emissions from the 4-injection baseline. As was observed for ϕ_c, some other minor trends were observed. The HC emissions increased when the ELSR was adjusted from baseline (50%-50%) to 70%-30% due to less favorable fuel stratification and an insufficiently fuel-rich region near the spark plug. The change of LLSR from the baseline (50%-50%) to 70-30% led to significant HC emissions increases. Though more fuel injected in the compression stroke managed to evaporate, less fuel being injected near TDC led to deteriorated in-cylinder gas-phase fuel distributions, worse combustion, lower ϕ_c and additional HC emissions. The ELSR LLSR adjustment can be a possible strategy to optimize the individual cold start combustion events. However, reaching the optimal late-late split ratio is not straightforward, and may depend on the cold start FRP and/or injected equivalence ratio.

Normalized HC emission results

To gain a better understanding of what a desirable cold start operational point would be, an emissions indicator labeled normalized HC emissions was defined as the experimentally obtained cold start emitted HC mass normalized by the average IMEP of all four cylinders for the first firing cycle. This represents the HC emissions for a given amount of indicated torque generated. This definition of "normalized HC emissions" reflects the idea that while HC emissions should be minimized, the ability of the engine to start should not be compromised.

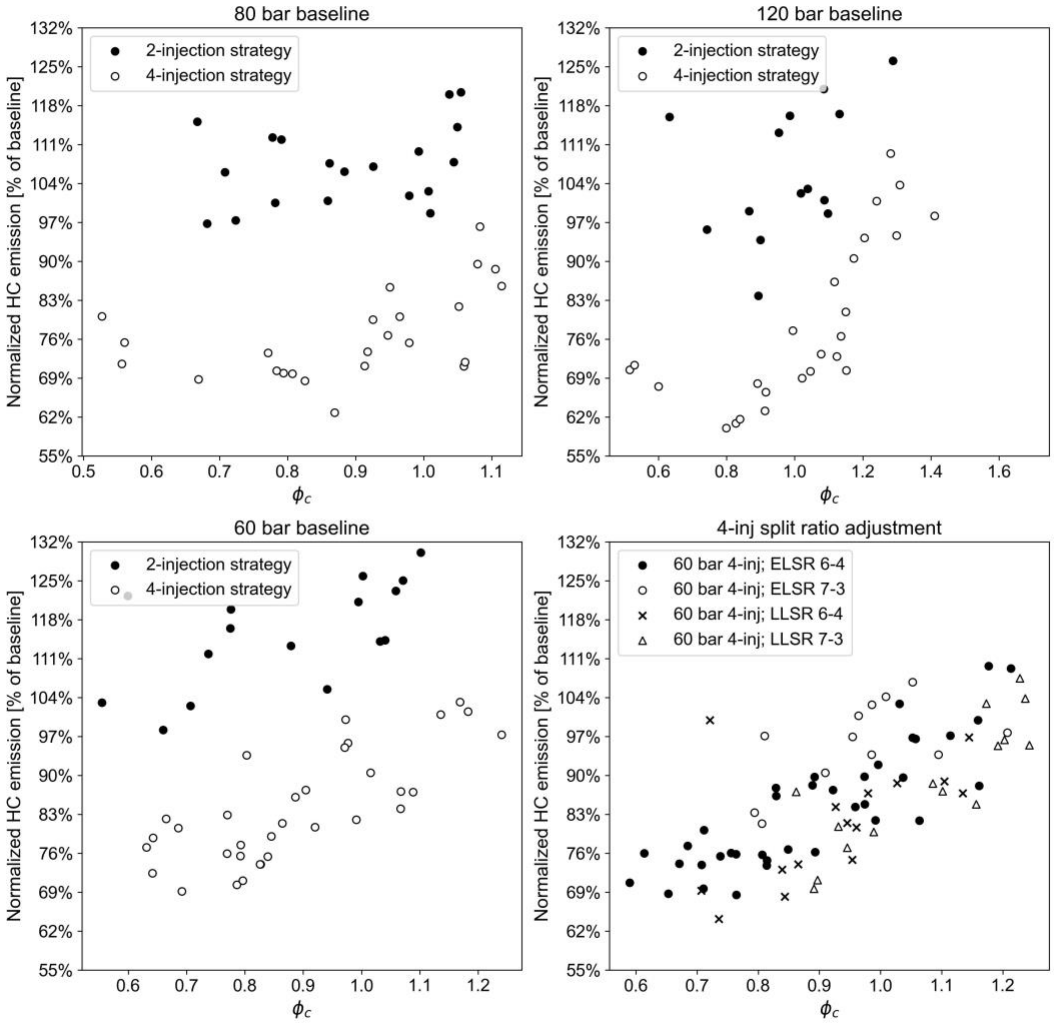

Figure 10 Normalized HC emissions versus combusted equivalence ratio, for 2-injections (a) and 4-injections (b) for different fuel rail pressures, 4-injections for different early-late fuel split (c), 4-injections for different late-late fuel split (d)

The normalized HC emissions data are plotted against the combusted equivalence ratio in Figure 10. The trends indicate a nearly constant or decrease in the normalized HCs as the combusted equivalence ratio increased from ~0.6 to 0.9 before increasing. Within the scatter of the data, the results show that both increasing the FRP and changing the injection strategy from 2- to 4-injections improved the overall HC emissions-energy release performance as reflected by the lower normalized HC emissions. Changing the split ratios, either ELSR or LLSR did not significantly affect the normalized HC emissions. The reduction achieved by switching from the 2- to the 4-injection strategy was more significant than the reduction from increasing FRP from 60 bar to 80 bar (and even more so relative to 120 bar). It is also worth pointing out that all

injection strategies had their normalized HC emissions minima located at approximately ϕ_c of 0.8. While it was initially thought it would be most desirable to achieve stoichiometric combustion during cold start, it was found that a relatively lean combusted equivalence ratio gave the best overall compromise between emissions and performance.

Numerical simulation results

Simulations using Converge CFD were used to analyze the two injection strategies in more detail. Details regarding how the simulations were carried out can be found in reference 21. The novel feature of the numerical simulation model was that it managed to simulate the cylinder mixing and combustion events with transient engine speeds. Validation of the numerical simulation results was carried out by comparing the simulation results with multiple cylinder pressure curves obtained from multiple repeated cold starts using the same group of powertrain parameters. The purpose of the repeated experiments was to include the potential event-by-event variations. As shown in Figure 11, the simulated cylinder 3 pressure curve using the 4-injection strategy closely follows the experimental data except for one event which experienced a partial burn. The simulation model managed to provide valid pressure curve profiles for the transient engine speed and was further used for engine fuel analysis. Readers are encouraged to refer to reference 15 for a more detailed introduction of the modeling and validation process.

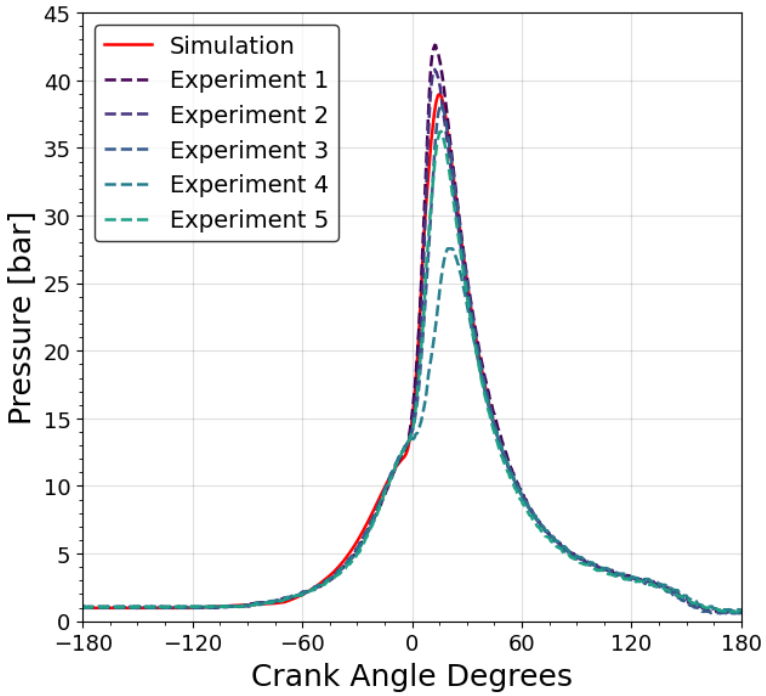

Figure 11 Comparison between pressure curves of cylinder 3 in the first firing event between simulation and experimental data

Simulations indicate that the average equivalence ratio in the combustion chamber at the time of ignition was 1.0 using the baseline 4-injection strategy, while it was only 0.84 using the 2-injection strategy with the same fuel mass injected per cylinder per cycle, which means more fuel

evaporated in the 4-injection strategy. The fuel evaporation had two sources, droplet evaporation and fuel film evaporation from surfaces. A leaner surrounding mixture along the paths of the 2nd injection for the early/late injection case assisted the process of fuel evaporation; the impacting droplets from the 1st injection had a greater fraction of the impacting fuel rebound from the surface, which led to more evaporation, as well. The surface film evaporation was also faster using the 4-injection strategy. Due to the different piston heights at the 4 different injection timings, the injected fuel had a chance to collide with a greater fraction of the piston surface, which resulted in more wetting area, but thinner wall films, aiding evaporation. These points are elaborated on in the previous reference.

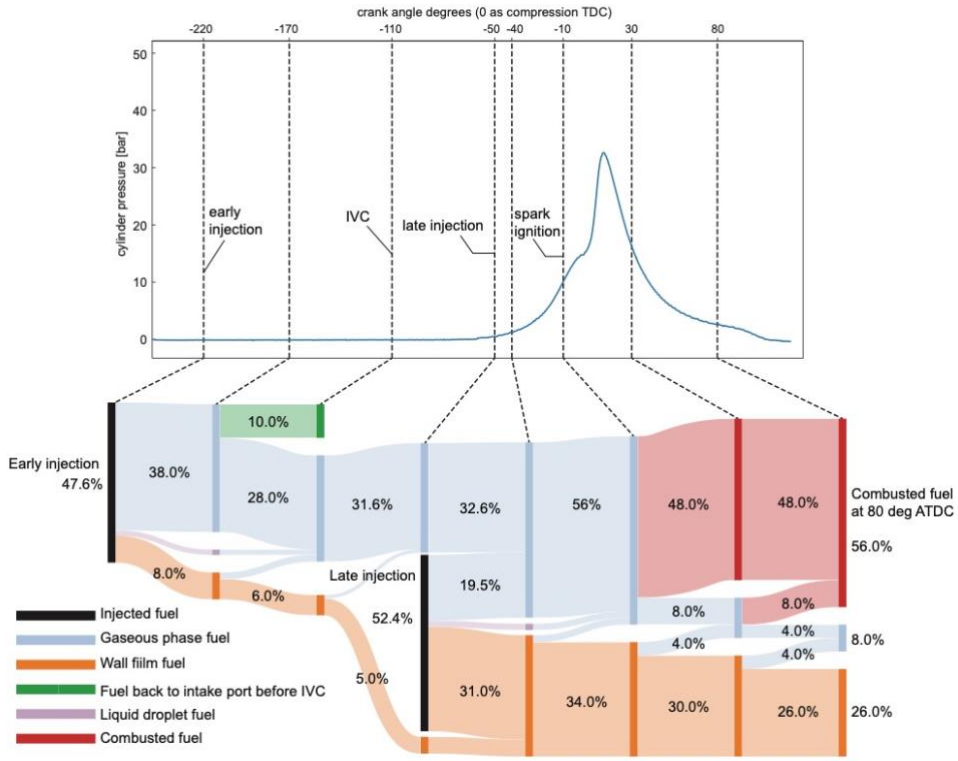

Figure 12 Sankey graph of the cold start fuel in cylinder 3 using the baseline 2-injection strategy**,** based on the simulations

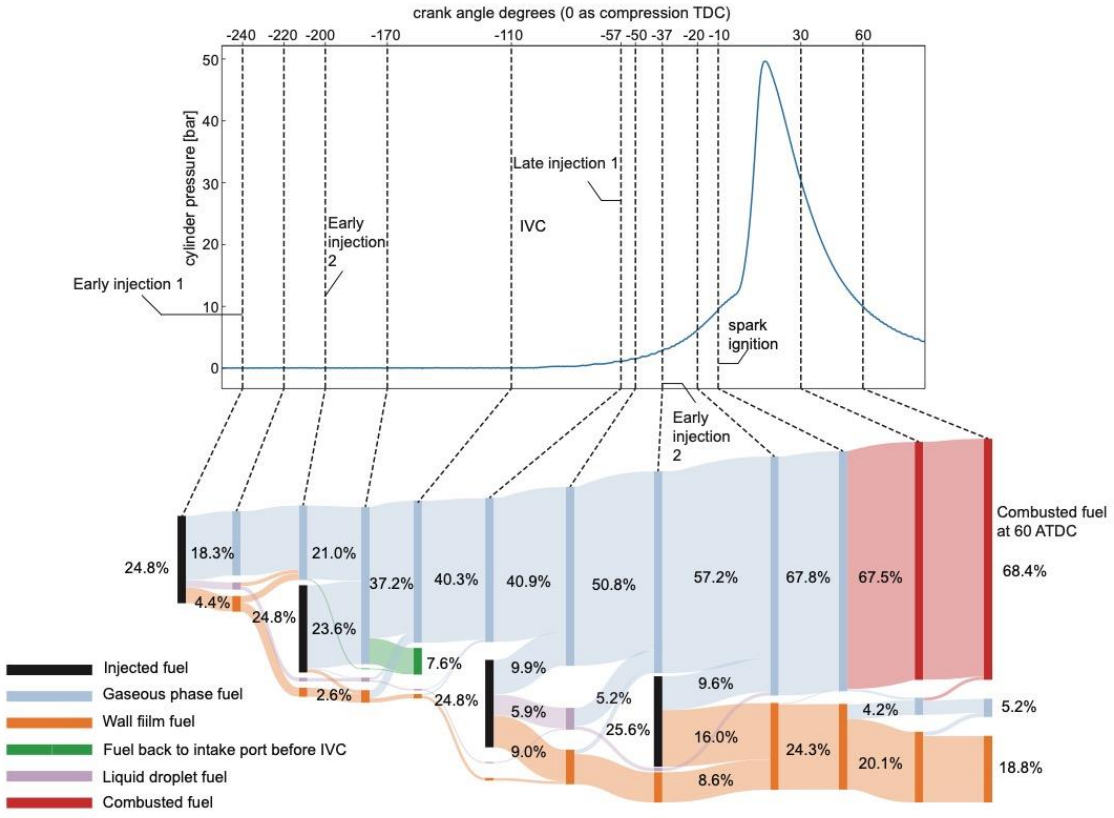

Figure 13 Sankey graph on the cold start fuel in cylinder 3 using the baseline 4-injection strategy, based on the simulations

Shown in Figure 12 and Figure 13 are two Sankey graphs which provide greater insight into the fate of the injected fuel and how it is partitioned among the different sinks for the 1st firing event of cylinder 3, according to the Converge simulation results. The baseline 2- injection strategy result, shown in Figure 12, should be compared with the baseline 4-injection strategy shown in Figure 13. The fuel rail pressure was 80 bar in both cases and the total injected mass was the same. It can be observed that the 4-injection case achieved greater evaporation of the fuel injected in both the intake stroke and compression stroke. For the fuel injected during the intake stroke, 2 early injections result in less wall wetting.

An interesting observation from the simulations is that a significant fraction of the gas-phase fuel from the intake stroke injections flows back into the intake port prior to IVC. This may affect the mixture in subsequent cycles and may even carry over to adjacent cylinders. The intake backflow amount was 10% of the early injected fuel for the 2-injection case, but only 7.6% for the 4-injection case.

For compression stroke injections, 2 late injections allow more fuel from the first compression stroke injection to evaporate. As a result, by the time of spark ignition, ~67.8% of the total injected fuel is in the gas phase and almost all of the gas phase fuel is combusted in the 4-injection case. In contrast, only 56% of the fuel is in the gas phase by the time of spark ignition in the 2- injection case, and the mixture stratification is less favorable such that the combustion is weaker, and the gas-phase fuel is not completely combusted until 30 degrees after TDC. The simulation results illustrated by the Sankey graphs are consistent with the experimental

observations discussed above, implying that the 4-injection strategy achieved better evaporation, formed a mixture that was more favorable for fast combustion, and led to higher energy release and less residual gas-and liquid-phase fuel converted to cold start HC emissions. By 80 degrees after TDC the simulations have 26% of the injected fuel still in the liquid-phase for the 2-injection case, versus 18.8% for the 4-injection case; this fuel is either lost to the crankcase or volatized later in the cycle and emitted as unburned hydrocarbons.

Conclusions

A parametric study was carried out to understand the effect of various powertrain parameters on GDI engine cold start HC emissions during the first firing cycle, where the engine speed, fuel rail pressure and cylinder temperature go through drastic transition. The study was carried out on a Ford 2.0 liter gasoline GDI engine using NI LabVIEW engine control software developed in-house and a custom gas collection analysis system. The parameters being studied included injected equivalence ratio, fuel rail pressure, number of injections, injection timing and injection split ratio. Both experimental and numerical simulation studies were carried out. The following conclusions were derived from this research.

1. The unburned HC emission mass from this GDI engine is attributed primarily to the incomplete evaporation of the fuel in the first firing cycle. Some of the unevaporated fuel is emitted from subsequent post-cold start cranking while a portion is also lost to the crankcase. To reduce HC emissions, it is essential to promote evaporation of the fuel and its rapid mixing with air to achieve combustion of as much of the injected fuel as possible. Contributing factors include the influence of puddle sizes and the accuracy of fueling and maintaining optimal combustion equivalence ratio for subsequent combustion cycles. Lower puddle masses should also make the air/fuel ratio less sensitive to changes in MAP (i.e., from fuel evaporating from puddles).
2. The calculated combusted equivalence ratio is well correlated with IMEP and CO_2 emissions regardless of other parameters, indicating that it is an important indicator of the combustion quality and the released energy.
3. Increasing fuel rail pressure (FRP) was found to improve fuel evaporation, leading to higher IMEP. On the other hand, FRP has a complicated effect on the HC emissions. Increasing FRP from 60 bar to 80 bar slightly decreased HC emissions for the 4-injection case but had no effect for 2-injections. Further, increasing the FRP to 120 bar from 80 bar increased the HC emissions by ~8.5% and ~6% for 2- and 4-injections, respectively.
4. Increasing the number of injections during the cycle from 2 to 4 improved the evaporation and combustion significantly. The 4-injection strategy gave higher IMEP and lower HC emissions given the same mass of fuel injected and the same FRP. For fuel rail pressures of 60, 80, and 120 bar, the baseline 4-injection strategy gave ~26%, ~21% and ~18% higher average IMEP and 6.5%, 11.9%, and 13.4% lower cold-start emitted HCs compared with the 2-injection strategy. Such phenomena could be explained by better overall fuel evaporation and more uniform fuel-air mixing that allowed additional-evaporated fuel to be combusted. The differences between the combusted fuel with injected equivalence ratios provided additional insights for the extent of fuel evaporation and degree of combustion for the various injection scenarios.

5. The normalized HC emissions, that is the cold start HC mass normalized by the cylinder IMEP was identified as a key indicator for performance where a favored smaller value was achieved with 4-injections rather than 2-injections and with higher FRP.
6. The 4-injection strategy improved combustion and reduced the HC emissions by 2 mechanisms: better evaporation and better fuel stratification. The greater extent of fuel evaporation allowed stronger, more extensive combustion and gave higher IMEP and slightly lower HC emissions given the same mass of fuel injected using the same FRP, lowering the normalized HC emissions. The simulations predicted gas-phase fuel mass at the time of ignition was 67.8% for the 4-injections case, but only 56% for the 2-injections case.
7. The lowest values for the HC emissions normalized by IMEP were observed for a lean combusted equivalence ratio of approximately 0.8.

Acknowledgments

This project was made possible through the funding provided by the Ford Motor Co. through the University of Texas at Austin's Site of the NSF Center for Efficient Vehicles and Sustainable Transportation Systems (EV-STS).

We wish to thank CONVERGE CFD™ for providing us with licenses for their simulation software and for their generous technical support.

The Texas Advanced Computing Center (TACC) of the University of Texas at Austin provided the computational resources for the simulations. Those simulations would not have been possible without their continued support.

References

1. Khameneian AA, Irdmousa BK, Dice P, Shahbakhti M, Naber JD, Moilanen P, Archer C, Glugla C, and Huberts G. A dynamic method to analyze cold-start first cycles engine-out emissions at elevated cranking speed conditions of a hybrid electric vehicle including a gasoline direct injection engine. *SAE Int. J. Engines* 2022, *15*(6). Epub ahead of print August 2022. DOI: https://doi.org/10.4271/03-15-06-0044.
2. Queiroz C, and Tomanik E. Gasoline direct injection engines - a bibliographical review. SAE Paper 973113. 1997. https://doi.org/10.4271/973113.
3. United States Environmental Protection Agency. *The 2021 EPA Automotive Trends Report: Greenhouse Gas Emissions, Fuel Economy, and Technology since 1975*. https://nepis.epa.gov/Exe/ZyPDF.cgi?Dockey=P1013L1O.pdf (November 2021, accessed 29 April 2022).
4. Tong K, Quay BD, Zello JV, and Santavicca DA. Fuel volatility effects on mixture preparation and performance in a GDI engine during cold start. SAE Paper 2001-01–3650. 2001. https://doi.org/10.4271/2001-01-3650
5. Peckham MS, Finch A, and Campbell B. Analysis of transient HC, CO, NOx and CO2 emissions from a GDI engine using fast response gas analyzers. *SAE Int J Engines* 2011; *4*(1): 1513–1522. https://doi.org/10.4271/2011-01-1227.

6. Fedor W, Kazour J, Haller J, Dauer K, and Kabasin D. GDi cold start emission reduction with heated fuel. SAE Paper 2016-01–0825. 2016. https://doi.org/10.4271/2016-01-0825
7. Wiemer S, Kubach H, and Spicher U. Investigations on the start-up process of a DISI engine. SAE Paper 2007-01–4012. 2007. https://doi.org/10.4271/2007-01-4012.
8. Yusuf AA, and Inambao FL. Effect of cold start emissions from gasoline-fueled engines of light-duty vehicles at low and high ambient temperatures: Recent trends. *Case Studies in Thermal Engineering* 2019; *14*: 100417.
9. Burke D, Foti D, Haller J, and Fedor W. Fuel rail pressure rise during cold start of a gasoline direct injection engine. SAE Paper 2012-01–0393. 2012. https://doi.org/10.4271/2012-01-0393
10. Bruno BA, Santavicca DA, and Zello JV. Fuel injection pressure effects on the cold start performance of a GDI engine. SAE Paper 2003-01-3163. 2003.. https://doi.org/10.4271/2003-01-3163.
11. Xu Z, Yi J, Wooldridge S, Reiche D, Curtis EW, and Papaioannou G. Modeling the cold start of the Ford 3.5L V6 EcoBoost engine. *SAE Int J Engines* 2009; *2*(1): 1367–1387. https://doi.org/10.4271/2009-01-1493
12. Rodriguez JF, and Cheng WK. Effect of operation strategy on first cycle CO, HC, and PM/PN emissions in a GDI engine. *SAE Int. J. Engines* 2015; *8*(3): 1098–1106. https://doi.org/10.4271/2015-01-0887
13. Fan Q, Bian J, Lu H, Li L, and Deng J. Effect of the fuel injection strategy on first-cycle firing and combustion characteristics during cold start in a TSDI gasoline engine. *Int. J Automot. Technol.* 2012; *13*: 523–531. https://doi.org/10.1007/s12239-012-0050-3
14. Fan Q, and Li L. Transient characteristics of cold start emissions from a two-stage direct injection gasoline engines employing the total stoichiometric ratio and local rich mixture start-up strategy. SAE Paper 2012-01–1068. 2012. https://doi.org/10.4271/2012-01-1068
15. Rodríguez JF, and Cheng WK. Fuel carbon pathway in the first cranking cycle of a gasoline direct injection engine. *Int. J. Engine Res.* 2016; *17*(6): 690–701. https://doi.org/10.1177/1468087415609852
16. Rodriguez JF, and Cheng WK. Cycle-by-cycle analysis of cold crank-start in a GDI engine. *SAE Int. J. Engines* 2016; *9*(2): 1210–1219. https://doi.org/10.4271/2016-01-0824
17. Rodriguez JF, and Cheng WK. Reduction of cold-start emissions through valve timing in a GDI engine. *SAE Int J Engines* 2016; *9*(2): 1220–1229. https://doi.org/10.4271/2016-01-0827
18. Hu J, Hall M, Matthews R, Moilanen P, Wooldridge S, and Yi J. A novel technique for Measuring cycle-resolved cold start emissions applied to a gasoline turbocharged direct injection engine. *SAE Int. J. Adv. & Curr. Prac. in Mobility* 2020; *2*(5): 2469–2478. https://doi.org/10.4271/2020-01-0312.
19. Malaguti S, Cantore G, Fontanesi S, Lupi R and Rosetti A. CFD Investigation of Wall Wetting in a GDI Engine under Low Temperature Cranking Operations. SAE Paper 2009-01-0704, 2009. https://doi.org/10.4271/2009-01-0704.
20. Hu J, Hall M, Matthews R, Moilanen P, and Wooldridge S. Quantitative analysis of gasoline direct injection engine emissions for the first 5 firing cycles of cold start. *SAE Int. J. Adv. & Curr. Prac. in Mobility* 2021, *3*(5):2384-2394. https://doi.org/10.4271/2021-01-0536.
21. Li D, Hu J, Hall M, and Matthews R. A simulation Study on the transient behavior of a gasoline direct injection engine under cold start conditions. SAE Paper 2022-01-0401, 2022. https://doi.org/10.4271/2022-01-0401.

22. Ravindran AC, Kokjohn SL, Petersen B. Improving computational fluid dynamics modeling of Direct Injection Spark Ignition cold-start. *Int. J. Engine Res*. 2021;22(9): 2786-2802. https://doi:10.1177/1468087420963982.
23. Ravindran AC, Kokjohn SL. Combining machine learning with 3D-CFD modeling for optimizing a DISI engine performance during cold-start. *Energy and AI* 2021;5: 100072. https://doi.org/10.1016/j.egyai.2021.100072.
24. Matthews RD, Hall MJ, Dai W, and Davis G. Combustion Modeling in SI Engines with a Peninsula-Fractal Combustion Model. *SAE J. Engines* 1996, *105*(3):80-195. https://doi.org/10.4271/960072.
25. Liu YD, Jia M, Xie MZ, and Pang B, Enhancement on a Skeletal Kinetic Model for Primary Reference Fuel Oxidation by Using a Semidecoupling Methodology," *Energy Fuels* 2012, 26(12):7069–7083. doi:10.1021/ef301242b.
26. Spindt RS. Air-Fuel Ratios from Exhaust Gas Analysis. SAE Paper 650507 (1965). https://doi.org/10.4271/650507.

Appendix: Mass-based equivalence ratio calculation

Given the measured mole fractions of CO2, CO, and HCs in the wet exhaust, the mass-based equivalence ratio was calculated as discussed below.

The gasoline was assumed to be standard gasoline with composition ($C_1H_{1.87}$). The combustion reaction equation was assumed to be:

$$nC_1H_{1.87} + m(O_2 + \alpha N_2 + \beta CO_2 + c\gamma H_2O) \rightarrow n_1CO_2 + n_2CO + (n_3C_1H_{1.87}) + n_4H_2O + n_5H_2 + n_6N_2 + n_7O_2$$

where α, β, and $c\gamma$ are all known relative concentration of nitrogen, carbon dioxide, and water vapor per mole of oxygen in air. For an accurate composition of air, α=3.72865, β is typically 0.001575, and c is a constant (7.6746×10^{-3}) that converts from the mass-based γ (the absolute humidity in $g_{H2O}/kg_{dry\ air}$) to the desired mole ratio and also converts from moles H_2O per mole of dry air to moles of H_2O per mole of the O_2 in air. The coefficients n, m and n_i (i=1, 2, …7) are all moles of the reactants and combustion products. The combustion equation assumes that no NO*x* is generated due to its very small (ppm) mole fraction. The HCs were assumed to be unburned fuel as $C_1H_{y/x}$, converted from the measured HCs in hexane. The moles of CO and CO_2 were obtained by processing the gas analyzer concentration data and the obtained exhaust gas volume. These assumptions left 6 unknown coefficients in the equation: n, m, n_i (i=4, 5, 6, 7).
To solve for all the unknowns, 6 equations were needed. The atom balance (mass conservation) equations for the 4 elements participating in the combustion reaction provide 4 of the required 6 equations in the 6 unknowns.

The carbon atom balance is:

$$n + m \cdot \beta = n_1 + n_2 + n_3$$

The hydrogen atom balance is:

$$1.87n + m \cdot 2c\gamma = 1.87n_3 + 2n_4 + 2n_5$$

The nitrogen atom balance is:

$$m \cdot 2\alpha = 2n_6$$

The oxygen atom balance is:

$$m(2 + 2\beta + c\gamma) = 2n_1 + n_2 + n_4 + 2n_7$$

The water-gas shift reaction equilibrium equation is frequently used in calculating the equivalence ratio and was applied here:

$$K = \frac{[\mathrm{CO}] \times [\mathrm{H_2}O]}{[\mathrm{CO_2}] \times [H_2]} = \frac{\mathrm{n_2} \times n_4}{\mathrm{n_1} \times n_5}, K = 3.5$$

The coefficient *K* was selected to be 3.5. This application of water-gas shift reaction was first used by Spindt[26].

The final equation assumed that the sum of all the product mole numbers is equal to the total gas mole emitted during the 1 firing cycle:

$$\sum_{i=1}^{7} n_i = \frac{pV}{N_{cyc}RT}$$

In the equation above, *p*, *T* and *V* are the pressure, temperature and the volume of the exhaust gas collected. N_{cyc} is the total number of cycles during emissions collection. and *R* is the universal gas constant.

After the unknowns are solved, the combusted equivalence ratio ϕ_c are solved by:

$$\lambda = \frac{m}{\left(1 + \frac{1.87}{4}\right) \times n}, \phi = \frac{1}{\lambda}$$